GeoScienceWorld
Lithosphere
Volume 2024, Article ID lithosphere_2023_103, 13 pages
https://doi.org/10.2113/2024/lithosphere_2023_103

Lithosphere

Research Article

Effects of Stress on Transport Properties in Fractured Porous Rocks

Jing Ba[1], **Jinyi Min**[1], **Lin Zhang**[1] and **José M. Carcione**[1,2]

[1]*School of Earth Sciences and Engineering, Hohai University, Nanjing, Jiangsu, 211100, China*
[2]*National Institute of Oceanography and Applied Geophysics – OGS, Borgo Grotta Gigante 42c, Trieste, Sgonico, 34010, Italy*

Correspondence should be addressed to Lin Zhang; zlin@hhu.edu.cn

Received 28 January 2023; Published 25 January 2024

Academic Editor: Guanglong Sheng

The nonlinear characteristics of the rock transport properties (permeability and electrical conductivity in this study) as a function of stress are closely related to the geometry of the pore space, which consists of stiff pores, microcracks, or microfractures. We consider two behaviors of the pore space, one linear and the other exponential, related to the stiff pores and microfractures, respectively, where the relation between stress and strain can be described by the Two-Part Hooke's Model. With this model, the relations between porosity, transport properties, and effective stress (confining minus pore pressure) can be obtained and validated with the experimental data of four tight sandstones collected from the Shaximiao Formation of Sichuan Basin, southwest China. The agreement is good. At low effective stresses, the closure of cracks is the main mechanism affecting the transport properties, whose behavior is similar in terms of their parameters. Subsequently, experimental data of nine tight sandstones from the Yanchang Formation, collected from the Ordos Basin, west China, are employed to confirm the previous results, indicating that the fluid and electrical current follow the same path in the pore space.

1. Introduction

Reservoir rocks have pores, cracks, or microfractures and are generally heterogeneous [1–4]. The deformation under loading is different in stiff pores and microfractures, which affects the elastic and transport properties, especially in low-permeability rocks. Since cracks provide a permeability path for the flow of reservoir fluids [5–9], understanding of the relationships between the transport properties and effective stress is important for detecting and monitoring reservoir fluids.

Previous studies revealed that the exponential function describes the behavior of permeability and conductivity as a function of effective stress [10–20]. However, an important point is to describe the behavior of the sharp decrease of these transport properties when the effective stress increases at low values, especially for low-permeability rocks [21, 22]. The power law has also been adopted to describe such variation [23–27]. For instance, Jones and Owens [28] and Walsh [29] reformulated the expression of power law. On the other hand, Kaselow and Shapiro [30] applied a four-parameter exponential equation to analyze the electrical conductivity as a function of the effective pressure.

The closure of cracks with increasing effective stress leads to lower porosity, and permeability or electrical conductivity shows a similar behavior. The transport properties as a function of porosity can be studied with a power law [31, 32] or by analyzing experimental data [21]. Archie [33] established an empirical relation between the formation factor (the ratio between bulk resistivity and that of water) and porosity. Subsequently, some researchers investigated the relationships between electrical conductivity and porosity [34, 35], clay content [36–38], crack radii, aspect ratios, tortuosity, and pore surface area [39–45].

Pores and cracks undergo different deformation under stress, and then the effects on porosity are different. A rock can be conceptually divided into "hard" and "soft" parts. By assuming that the cracks are homogeneously distributed in the rock, Two-Part Hooke's Model (TPHM) proposed by

Liu et al. [46], to characterize the stress–strain relations of porous and fractured rocks, indicates that cracks contribute nonlinearly. This nonlinear deformation may be the result of the combining effects of nonuniform pore size distributions and pore geometry heterogeneity [47]. Zheng et al. [22] derived the relations between porosity, permeability, and effective stress of low-permeability rocks based on this model and verified them by using experimental data. Based on these relations, Wu et al. [48] provided a stress-sensitivity method suitable for depletion mining and water-injection development processes. The satisfactory results are achieved by using the model [49–53]. In addition, Liu et al. [46] stated that the soft part also has an effect on the electrical conductivity, confirmed by Watanabe et al. [54] in the brine-saturated granite. They found that the closure of narrow apertures (i.e., cracks) leads to a sharp decrease in the conductivity. Pang et al. [55] studied the effects of pores, cracks, and clay content on elastic wave velocity and electrical conductivity by using an acoustical–electrical model. The aforementioned studies regarding the experimental measurements of electrical conductivity and rock physical models have analyzed the significant impacts of microcracks on electrical conductivity. However, it is still a challenge to establish a robust model in describing the contributions of pores and microcracks to electrical conductivity within the whole stress range. According to the work of Walsh and Brace [56], it is pointed out that the flow of fluid and electrical current in rocks are similar and follow similar migration paths, and other studies have shown that there is a correlation between permeability and electrical conductivity [57–59]. This means that the relationships between permeability and effective stresses (e.g., a power law relationship) may be extended to the case of conductivity. As an extension of the works of Liu et al. [46] and Zheng et al. [22], this study proposes to separate the effects of pores and microcracks on conductivity based on TPHM.

In this study, we analyze the relations between transport properties, porosity, and effective stress by using the TPHM, verified experimental data of tight sandstones from the Shaximiao Formation. The related parameters are further analyzed by data corresponding to tight sandstones collected from the Yanchang Formation. The theory can be used to establish cross-property relationship between permeability and resistivity [60].

2. Theory

2.1. Two-Part Hooke's Model. According to Liu et al. [46], a porous and fractured rock can be divided into "soft" and "hard" parts (Figure 1), where the former is composed of microcracks or microfractures with a large degree of relative deformation and follows the natural-strain-based Hooke's law, and the latter is the residual structure with less deformation and follows the engineering-strain-based Hooke's law. Let subscripts "e" and "t" refer to the hard and soft parts. For the soft part, the deformation corresponds to the natural strain, with the volume change scaled to the current pore volume, and the stress–strain relation of the soft part is

$$\frac{d\sigma}{K_t} = d\varepsilon_{v,t} = -\frac{dV_t}{V_t} \tag{1}$$

where K_t is the bulk modulus, σ is the effective stress (confining minus pore pressure), and V denotes volume. Integrating equations (1) with the initial condition $V = V_{0,t}$ for $\sigma = 0$, we have:

$$V_t = V_{0,t}\exp(-\frac{\sigma}{K_t}) \tag{2}$$

where subscripts "0" denote the unstressed state.

For the hard part, the deformation corresponds to the engineering strain, with the volume change scaled to the initial pore volume, and we have

$$\frac{d\sigma}{K_e} = d\varepsilon_{v,e} = -\frac{dV_e}{V_{0,e}} \tag{3}$$

where K_e is the bulk modulus. Integrating equations (3) with the initial condition $V_e = V_{e,0}$ for $\sigma = 0$, we obtain

$$V_e = V_{0,e}(1 - \frac{\sigma}{K_e}) \tag{4}$$

Therefore, the stress–strain relation is given by

$$\varepsilon = -\frac{dV}{V_0} = \gamma_e\frac{d\sigma}{K_e} + \gamma_t\exp(-\frac{\sigma}{K_t})\frac{d\sigma}{K_t} \tag{5}$$

where $V_0 = V_{0,t} + V_{0,e}$, $\gamma_t = V_{0,t}/V_0$, and $\gamma_e = 1 - \gamma_t$.

2.2. Porosity and Permeability. The total porosity of the rock is given by [46]

$$\phi = \phi_{e,0}(1 - C_e\sigma) + \gamma_{t,0}\exp(-\frac{\sigma}{K_t}), \tag{6}$$

where $C_e = 1/K_e$ is the compressibility for the hard fraction of the pore volume, $\phi_{e,0} + \gamma_{t,0} = \phi_0$, $\phi_e = \phi_{e,0}(1 - C_e\sigma)$ is the hard-part porosity, and $\phi_t = \gamma_{t,0}\exp(-\sigma/K_t)$ is the soft-part porosity.

Although the soft part represents extremely small, the apparent decrease in permeability at low-effective stresses is closely related to its deformation. Assuming that the soft-part permeability is $K_t = \alpha(\phi_t)^m$, where σ and m are constants, Zheng et al. [22] derived the following expression for the permeability:

$$k = k_{e,0}\exp[-\beta C_e\phi_{e,0}\sigma] + \alpha[\gamma_{t,0}\exp(-\frac{\sigma}{K_t})]^m, \tag{7}$$

where $k_{e,0}$ is the hard-part permeability under an unstressed condition, and β is a constant (i.e., a stress-sensitive coefficient).

Due to experimental limitations, a measurement at zero effective stress (index "0") cannot be performed, and it is

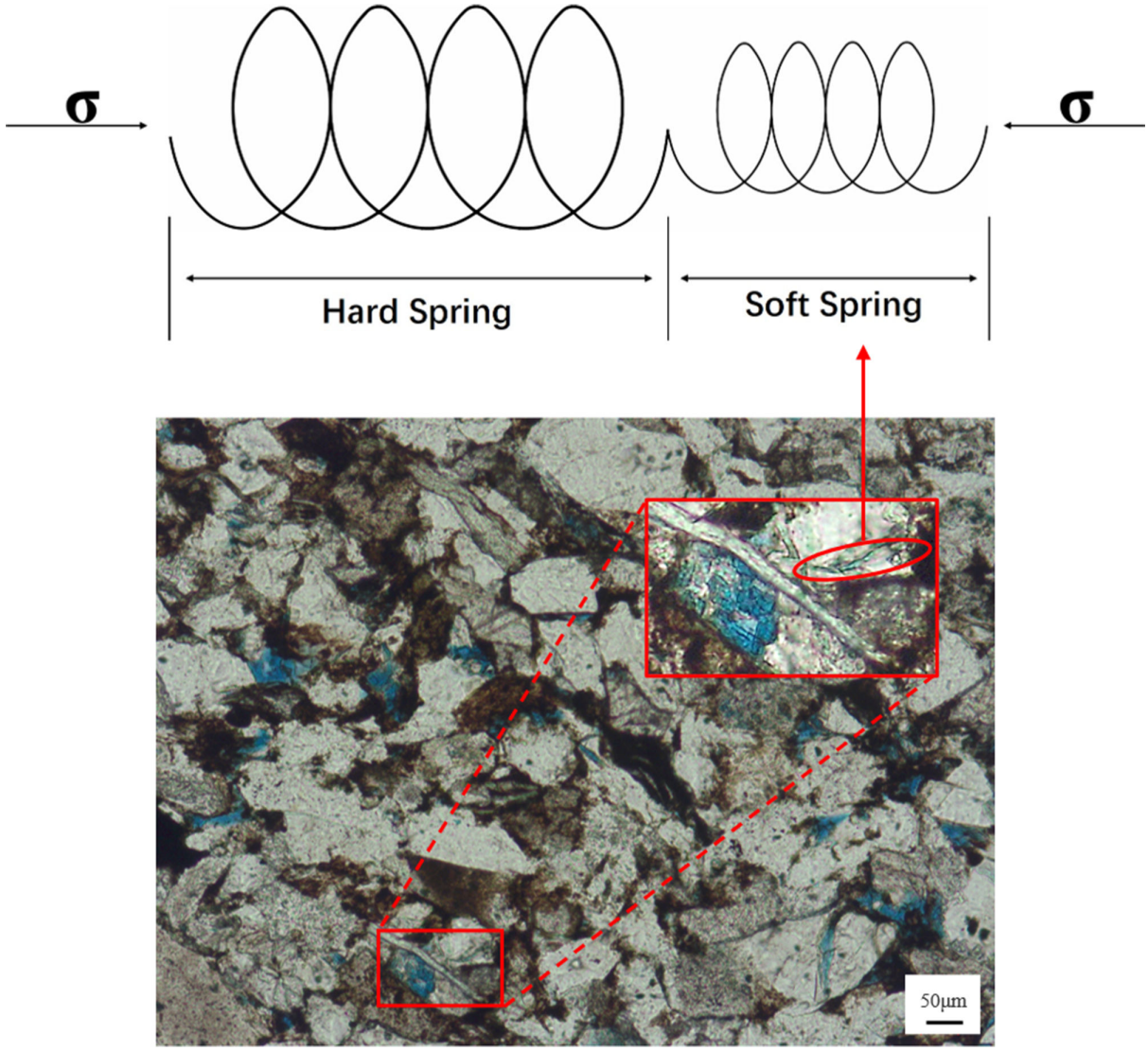

Figure 1: Two-Part Hooke's Model.

approximated by that at the minimum effective stress (index "1") [22]. Then, equations (6) and (7) are further reformulated as

$$\phi = \phi_{e,1}(1 - C_e\Delta\sigma) + \gamma_{t,1}\exp(-\frac{\Delta\sigma}{K_t}), \tag{8}$$

$$k = k_{e,1}\exp[-\beta C_e\phi_{e,1}\Delta\sigma] + \alpha[\gamma_{t,1}\exp(-\frac{\Delta\sigma}{K_t})]^m, \tag{9}$$

where $\Delta\sigma = \sigma - \sigma_1$, σ_1 is the minimum effective stress, $\phi_{e,1}$ and $k_{e,1}$ are the hard-part porosity and permeability at σ_1, respectively, and $\gamma_{t,1}$ is the soft-part porosity at σ_1.

2.3. Electrical Conductivity. The electrical conductivity of a rock is closely related to porosity [33, 61, 62], and cracks are the main cause of its nonlinear behavior [10, 35, 55]. Similarly, the variations of conductivity with effective stress are also attributed to the deformations of pores and cracks. By assuming that the cracks are closed at high-effective stresses, their contributions to conductivity are negligible. Then,

$$d(\ln S_e)/d\sigma = a(1/V_0)(dV_e^p/d\sigma), \tag{10}$$

where S_e is the conductivity of the hard part, a is a constant, and $dV_e^p = -C_eV_{e,0}d\sigma$ [46]. This part is in accordance with the theory of poroelasticity. By integrating equation (10) with an initial condition of $S_e = S_{e,0}$ for $\sigma = 0$, we obtain

$$S_e = S_{e,0}\exp[-a\phi_{e,0}C_e\sigma], \tag{11}$$

where $S_{e,0}$ is the conductivity at an unstressed condition.

From the previous section, we note that the conductivity at low-effective stresses is mainly associated with the

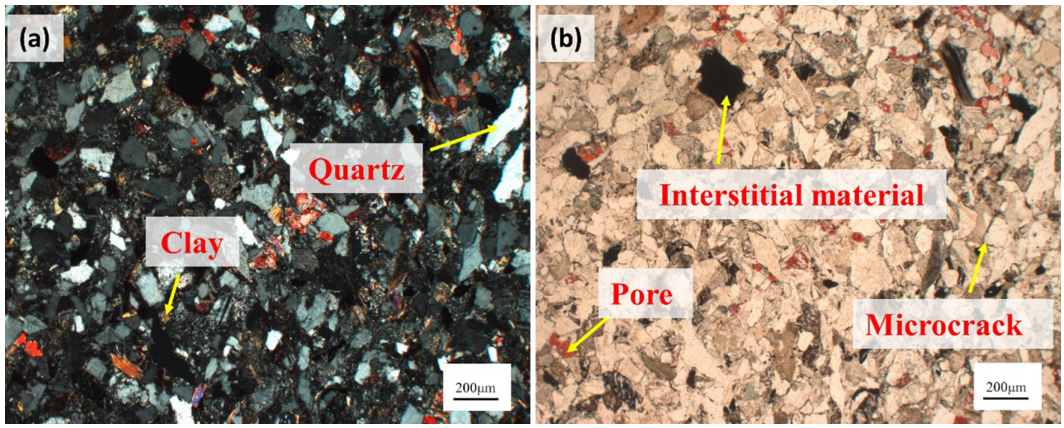

Figure 2: Thin sections of the TS4 sample. (a) Orthogonal polarization diagram. (b) Single polarization diagram.

Table 1: Properties of the Shaximiao Formation tight-sandstone samples.

Sample	Porosity (%)	Dry-rock density (kg/m^3)	Permeability (mD)	Clay (%)	Siderite (%)	Pyrite (%)
TS1	11.96	2340	0.7294	14.1	0.1	0.1
TS2	10.10	2390	0.2203	13.4	0.1	1.0
TS3	6.79	2470	0.1705	11.7	0.2	0.3
TS4	3.90	2550	0.0268	-	-	-

large relative deformation of cracks. The conductivity of the soft part is then obtained by subtracting S_e from the total conductivity,

$$S_t = S - S_e. \tag{12}$$

Similar to Zheng et al. [22], a power law function is adopted to describe the empirical relationship between conductivity and soft porosity, that is,

$$S_t = b[\phi_t]^n, \tag{13}$$

where b and n are constants. By combining equations (11), (12), and (13), we obtain the bulk conductivity as

$$S = S_{e,1}\exp[-a\phi_{e,1}C_e\Delta\sigma] + b[\gamma_{t,1}\exp(-\frac{\Delta\sigma}{K_t})]^n, \tag{14}$$

where $S_{e,1}$ is the hard-part conductivity at σ_1, and we have considered the minimum effective stress (index "1"). Comparison between equations (9) and (14) shows that the expressions of conductivity and permeability are similar, as illustrated in previous studies [57].

3. Experimental Data

3.1. Samples. We have measured the properties of four tight-sandstone samples from the Jurassic Shaximiao Formation of Sichuan Basin, China as a function of effective stress. The porosity has been obtained with the helium expansion method, and the permeability was determined with the unsteady-state pulse transient decay technique. An impedance–capacitance–resistance meter was used to measure the electrical conductivity with brine saturation (5% concentration). Porosity and permeability are measured at the range of 2–58 MPa, and conductivity is measured at the range of 5–35 MPa. The properties are given in Table 1. Figure 2 shows thin sections of the TS4 sample, a lithic feldspar sandstone with mostly pore-contact cementation. The mineral composition is mainly quartz, with feldspar and rock fragments, and the interstitial materials include clays and calcite. Additionally, a small amount of metallic minerals, such as siderite and pyrite, can be observed.

3.2. Verification of the Porosity and Permeability Equations. Figures 3 and 4 compare the theoretical (equations (8) and (9)) and experimental porosity and permeability of the four tight sandstones as a function of effective stress, respectively. At low stresses, the properties decrease nonlinearly, followed by a linear trend at high stresses. The nonlinear deformation under low stress may be caused by the closure of the slot-like cracks corresponding to the soft part. The porosity (permeability) fitting coefficients R^2 of TS1–TS4 samples are 0.97 (0.98), 0.96 (0.96), 0.92 (0.85), and 0.97 (0.88), respectively. The method to obtain the fitting parameters (see Table 2) is that of Liu et al. [46] and Zheng et al. [22]. Specifically, at high stresses, there is a linear relation between $\log(k_e)$ and σ , which can fit with $k_e = k_{e,1}\exp[-\beta C_e\phi_{e,1}\Delta\sigma]$. Then, the slope $-\beta C_e\phi_{e,1}$ of the straight line can be used to estimate the value of β, where the values of C_e and $\phi_{e,1}$ have been obtained by fitting the porosity-stress data. The value of $k_{e,1}$ is determined by

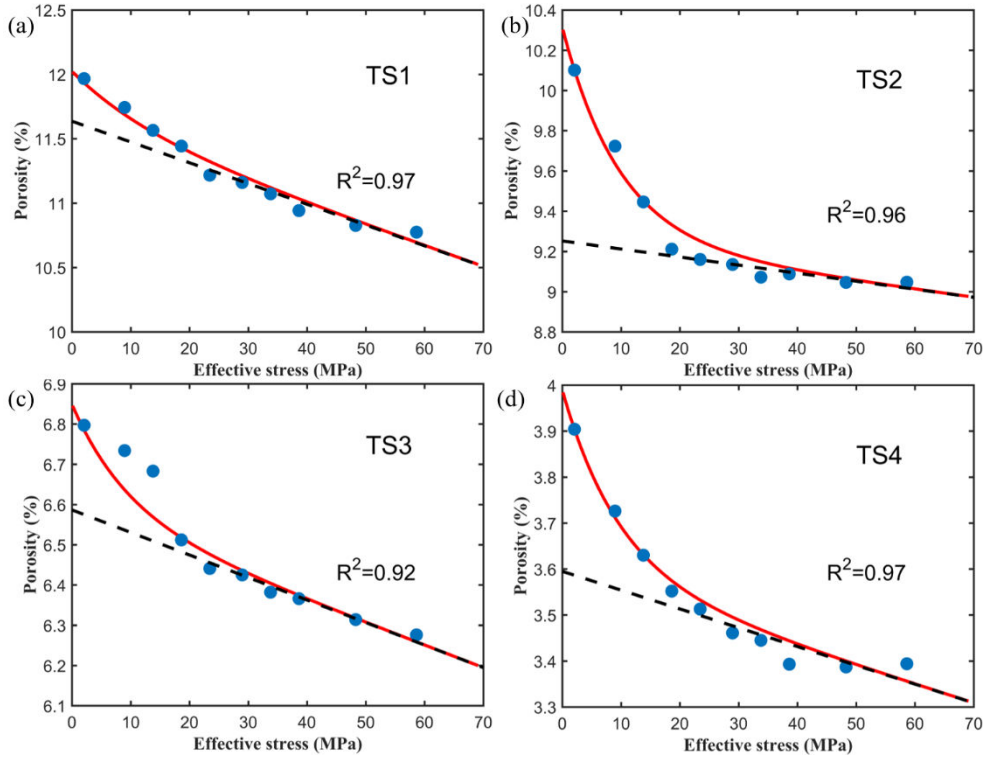

FIGURE 3: Porosity as a function of effective stress for (a) TS1, (b) TS2, (c) TS3, and (d) TS4. The red curves are the fitting results of equation (8), the black dotted curves are the results of the hard-part porosity, and the dots are the experimental data.

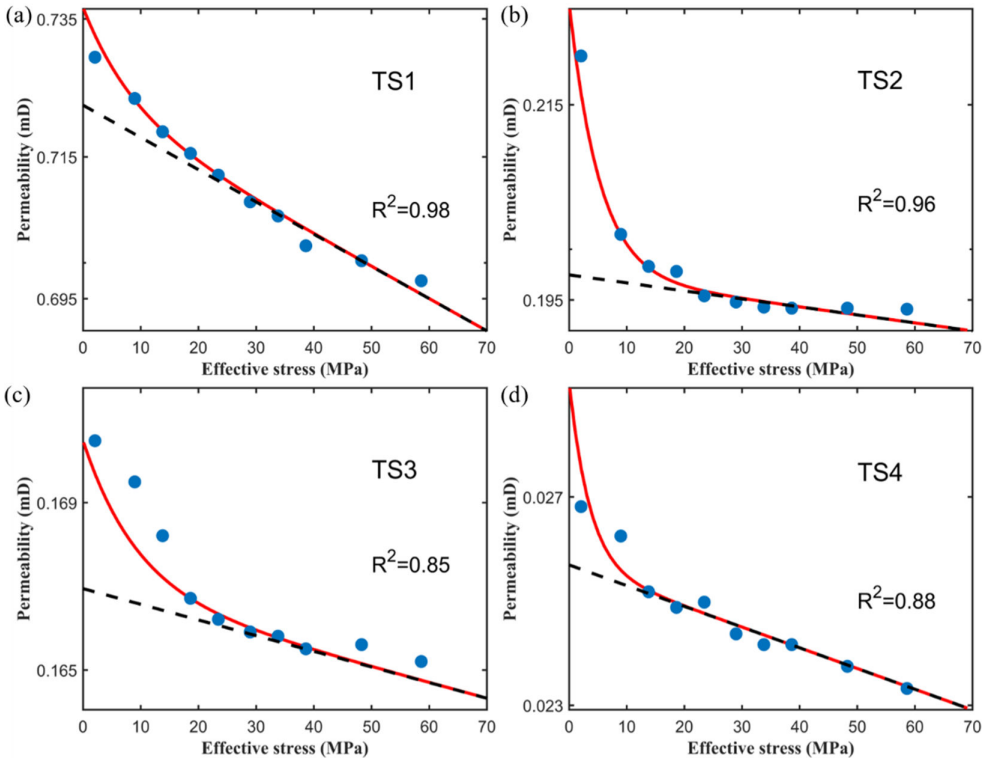

FIGURE 4: Logarithm of the permeability as a function of the effective stress for (a) TS1, (b) TS2, (c) TS3, and (d) TS4. The red curves are the fitting results of equation (9), the black dotted curves are the results of the hard-part data, and the dots are the experimental data.

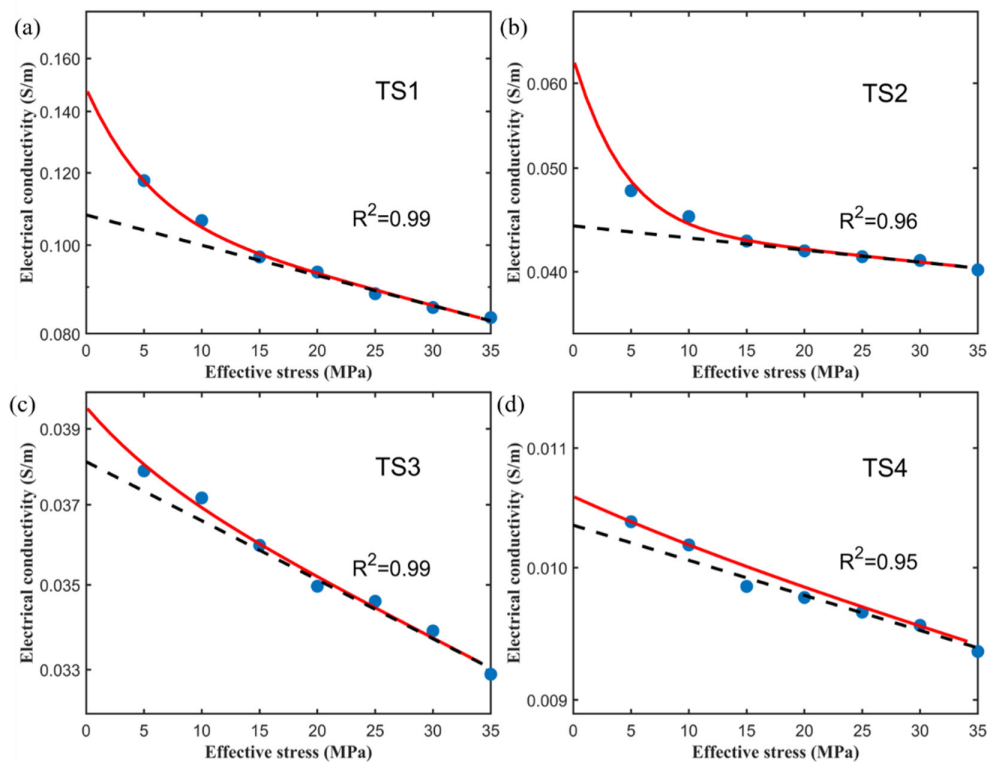

FIGURE 5: Logarithm of the conductivity as a function of the effective stress for (a) TS1, (b) TS2, (c) TS3, and (d) TS4. The red curves are the fitting results of equation (14), the black dotted curves are the results of the hard-part data, and the dots are the experimental data.

TABLE 2: Fitting parameters corresponding to the Shaximiao tight-sandstone samples.

	$\Phi_{e,1}$ (%)	C_e (MPa^{-1})	$\gamma_{t,1}$ (%)	K_t (MPa)	$k_{e,1}$ (mD)	β	α (mD)	m	a	b (S/m)	$S_{e,1}$ (S/m)	n
TS1	11.60	1.39E-03	0.33	13.14	0.72	0.04	0.06	1.57	0.47	0.60	0.11	2.85
TS2	9.24	4.33E-04	0.86	9.67	0.20	0.10	0.03	1.95	0.65	0.02	0.04	2.58
TS3	6.58	8.52E-04	0.21	9.29	0.17	0.04	0.01	1.02	0.73	0.01	0.04	1.37
TS4	3.59	1.14E-03	0.32	9.51	0.02	0.39	0.06	2.86	0.68	0.01	0.01	0.62

extrapolating the straight line at σ_1. The soft-part permeability can be obtained by using $k_t = k - k_e$, and the values of α and m can be estimated according to $k_t = \alpha(\phi_t)^m$.

Table 2 shows that the soft-part porosity of sample TS2 is the largest, while that of sample TS3 is the smallest. This indicates that TS2 experiences the largest decrease in porosity and permeability at low stresses. On the contrary, TS3 has the smallest decrease in these properties. Porosity and the permeability logarithm as a function of stress are linear at high stresses, indicating that the contribution of the soft part can be neglected at this range. Furthermore, the high-stress range can be set as 20–58 MPa, and 2–15 MPa can be defined as a low range, which may be used for the parameter estimation of the soft part.

3.3. Verification of the Electrical Conductivity Equation. Figure 5 shows the results for the electrical conductivity. Similar to the porosity and permeability, the conductivity decreases nonlinearly with stress. However, this behavior is not evident for sample TS4, and constant n corresponding to the soft part is significantly smaller than that of the other samples (see Figure 6). There are fewer TS3 and TS4 soft part data points. This is because microcracks or microfractures, like the soft part in TS3 and TS4, are likely to have a smaller aspect ratio, and the soft part will sharply decrease and gradually approach closure in the lower effective pressure range. The results of equation (14) agree with the experimental data, where the fitting coefficients R^2 of the four samples are 0.99, 0.96, 0.99, and 0.95. The conductivity variation is significant at low stresses, while at high stresses, cracks close and do not contribute to the fluid-flow continuity, showing a linear decreasing trend.

Similar to the permeability, the decrease of the soft-part porosity of TS2 is the largest at low stresses, while that of the TS3 sample is smaller. The results indicate that the soft part contributes as a major fluid migration path and cannot be neglected at low stresses. At high stresses, there is a linear relationship between $\log(S_e)$ and σ, which can be fitted with equation (11). Then, the slope $-aC_e\phi_{e,1}$ of the straight line can be used to estimate a, where the values of C_e and $\phi_{e,1}$

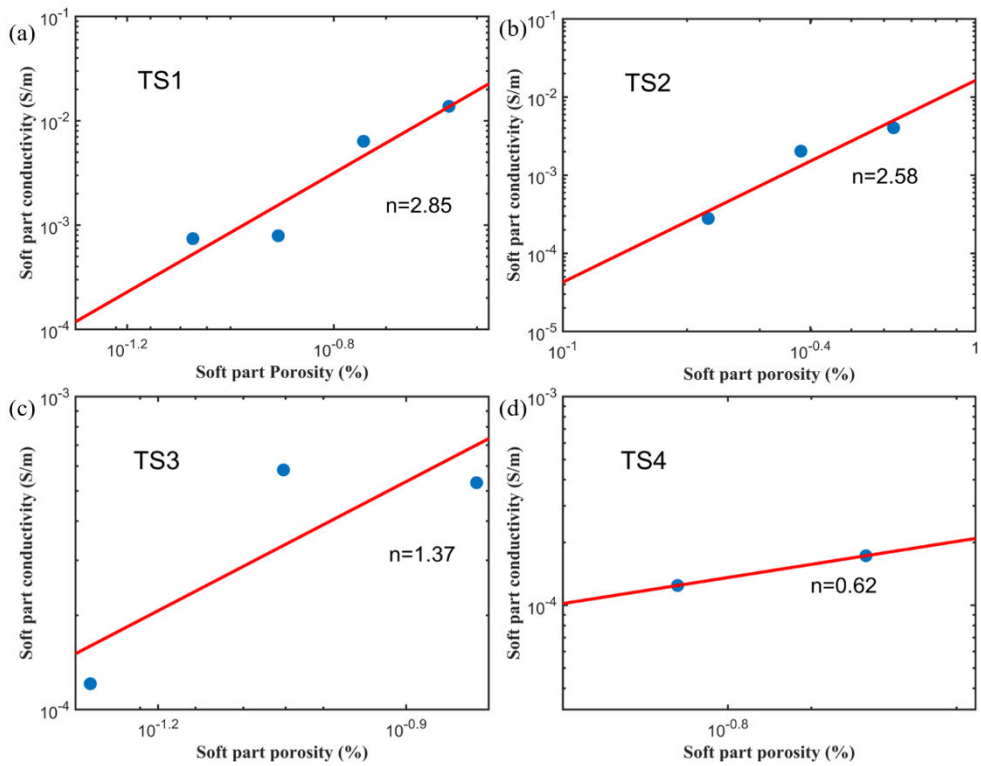

Figure 6: Soft-part conductivity as a function of the soft-part porosity for (a) TS1, (b) TS2, (c) TS3, and (d) TS4. The dots are the experimental data.

Table 3: Properties of the Yanchang Formation tight-sandstone samples.

Sample	Porosity (%)	Dry-rock density (kg/m^3)	Permeability (mD)	Clay (%)	Siderite (%)	Pyrite (%)
TS18	5.787	2510	0.020	7.84	1.19	-
TS19	6.156	2530	0.016	5.55	0.52	0.39
TS27	7.674	2470	0.074	5.19	0.75	-
TS30	8.791	2430	0.056	7.16	0.86	-
TS35	9.222	2410	0.066	5.35	0.75	-
TS38	10.165	2370	0.096	6.07	1.07	-
TS40	5.065	2440	0.018	5.59	0.54	-
TS41	7.259	2480	0.015	6.60	1.82	-
TS42	7.547	2460	0.043	4.34	1.80	0.17

have been obtained by fitting the porosity-stress data. The value of $S_{e,1}$ is determined by extrapolating the straight line at σ_1. The soft-part conductivity is obtained with equation (12), and then b and n can be estimated according to equation (13). The soft-part porosity and conductivity are shown in Figure 6, and the fitting parameters are listed in Table 2.

Table 2 shows that $\gamma_{t,1}$ accounts for a small part of the total porosity, and it decreases sharply with increasing stress. The soft-part bulk modulus K_t (9–13 MPa) is much smaller than that of a tight sandstone sample (29–31 GPa). Some parameters (C_e and K_t) have their own specific meanings and can be measured directly by laboratory experiments, but in this paper, they are calculated by fitting the experimental data. Moreover, Liu et al. [46] pointed out the rationality of the parameters such as pore compressibility and bulk modulus of soft part obtained by fitting calculation. Note that $k_{e,1}$ is significantly lower than the measurement at the minimum effective stress, which means that the soft-part permeability is the main contribution in this case. The value of m, obtained by fitting the permeability-porosity data, is between 1 and 2.86, with an average of 1.85, lower than that of the silty shale in Zheng et al. [22]. This is because the stress sensitivity of the latter is significantly higher [63]. Regarding the conductivity (unlike the TS4 sample), n ranges from 1.37 to 2.85, with an average of 2.26, close to m, indicating that the flow of fluid and electrical current follow similar migration paths [56]. Furthermore, the value of $S_{e,1}$ is much lower than the measurement

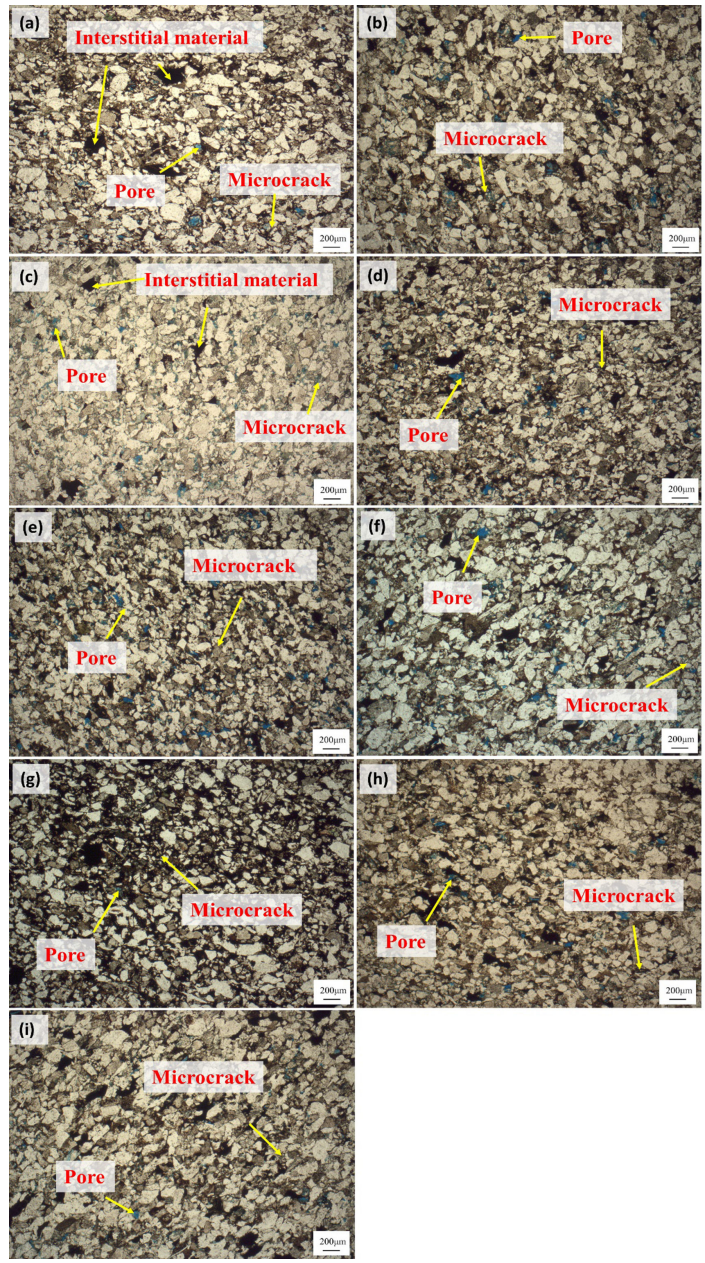

FIGURE 7: Single-polarization diagrams of the nine tight sandstones of the Yanchang Formation. (a) TS18 sample, (b) TS19 sample, (c) TS27 sample, (d) TS30 sample, (e) TS35 sample, (f) TS38 sample, (g) TS40 sample, (h) TS41 sample, and (i) TS42 sample.

at the minimum effective stress, suggesting that the soft-part conductivity also plays an important role. It should be noted that these fitting parameters can be affected by the selection of the stress range of the two parts.

3.4. Applications to Other Tight-Sandstone Samples. To verify the validity of equations (8), (9), and (14), based on the TPHM model, we consider nine tight-sandstone samples collected from the Member 7 of Yanchang Formation in Qingyang area, Ordos Basin, west China. According to X-ray diffraction and thin sections analysis, they mainly consist of quartz, feldspar, and clay. Their porosity and permeability are in the range of 5.065%–10.165% and 0.015–0.096 mD, respectively. They are typical low-permeability rocks, whose properties are given in Table 3. The porosity and permeability are measured by the automated permeameter of the Core Measurement System at stresses of 5–45 MPa, and the conductivity is measured with the two-electrode method at 3–45 MPa. Figure 7 shows thin sections of the samples, where pores and microcracks can be seen.

Figures 8–10 show the results for porosity, permeability, and conductivity, respectively. The results show that the theoretical equation based on the TPHM theory can provide a good agreement with the experimental data. At low stresses, the cracks play an important role. According to Tables 2 and 4, the values of m and n

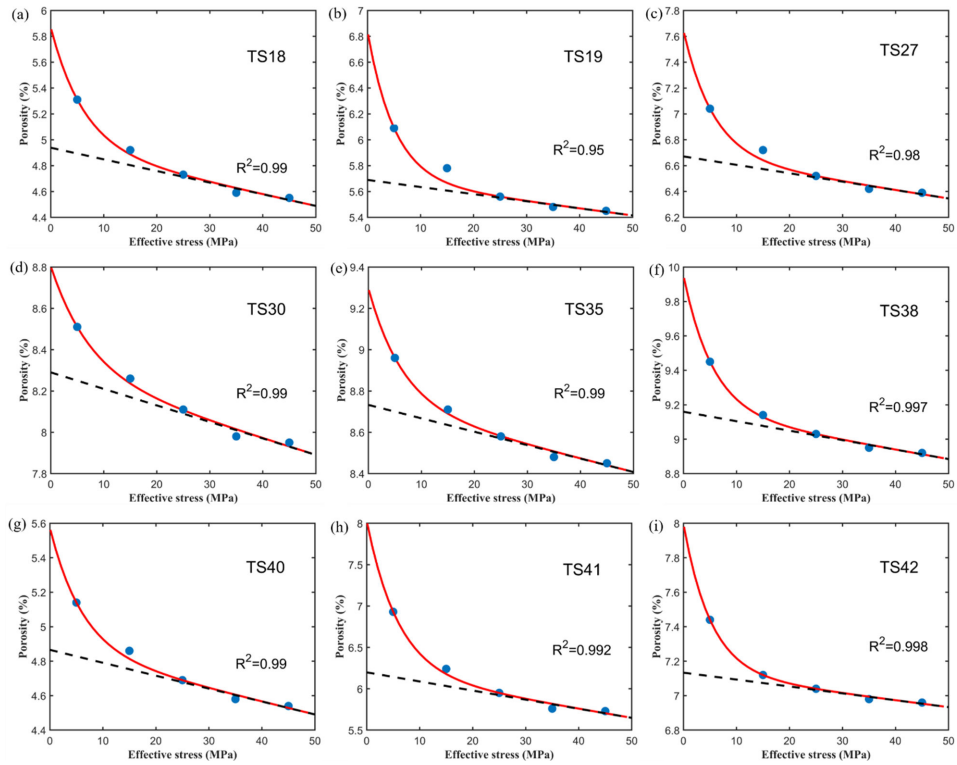

FIGURE 8: Porosity as a function of effective stress corresponding to the tight sandstones of the Yanchang Formation. (a) TS18, (b) TS19, (c) TS27, (d) TS30, (e) TS35, (f) TS38, (g) TS40, (h) TS41, and (i) TS42. The red curves are the fitting results of equation (8), the black dotted curves are the results of the hard-part data at high stresses, and the dots are the experimental data.

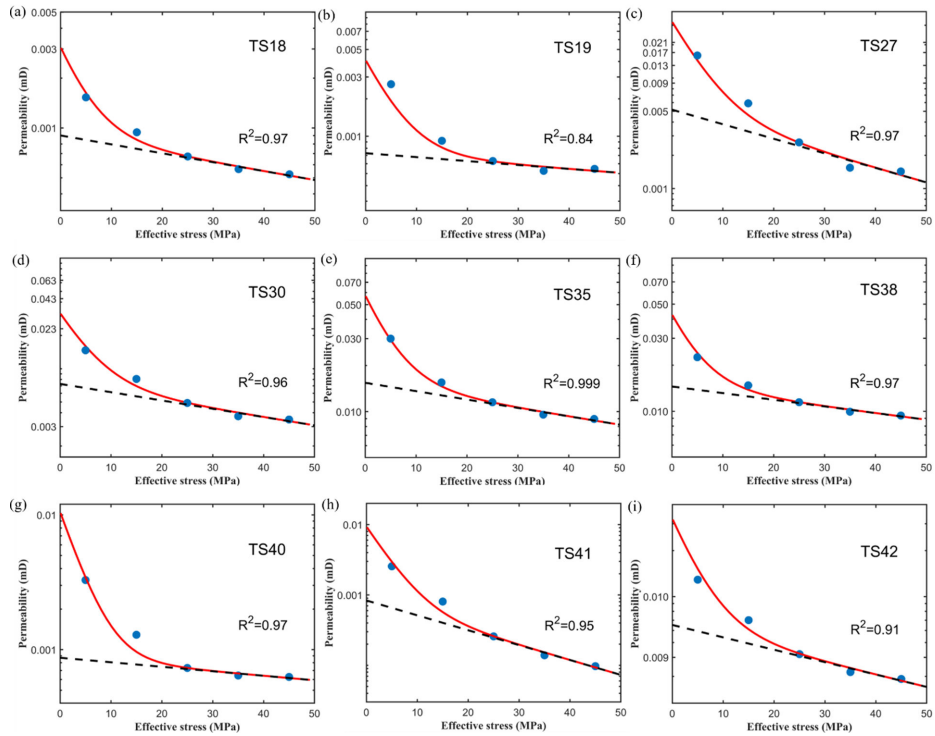

FIGURE 9: Logarithm of the permeability as a function of the effective stress corresponding to the tight sandstones of the Yanchang Formation. (a) TS18, (b) TS19, (c) TS27, (d) TS30, (e) TS35, (f) TS38, (g) TS40, (h) TS41, and (i) TS42. The red curves are the fitting results of equation (9), the black dotted curves are the results of the hard-part data at high stresses, and the dots are the experimental data.

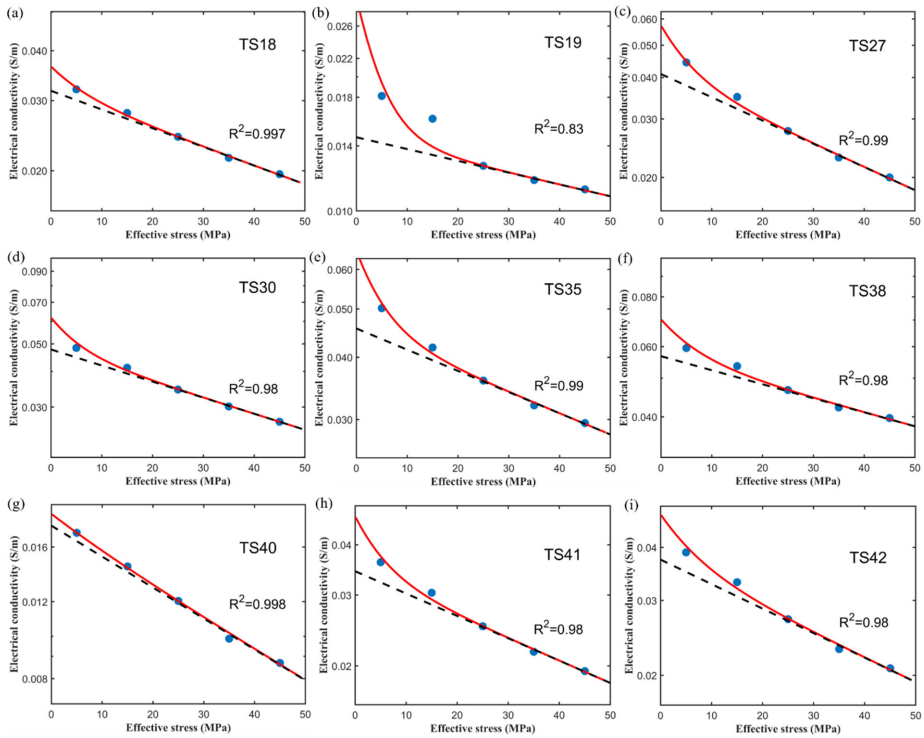

FIGURE 10: Logarithm of the conductivity as a function of the effective stress for the tight sandstones of the Yanchang Formation. (a) TS18, (b) TS19, (c) TS27, (d) TS30, (e) TS35, (f) TS38, (g) TS40, (h) TS41, and (i) TS42. The red curves are the fitting results of equation (14), the black dotted curves are the results of the hard-part data at high stresses, and the dots are the experimental data.

are also similar, so it might be possible to estimate conductivity from permeability and vice versa, by using this correlation.

4. Discussion

In general, conductivity increases with clay content [55, 64]. Comparing Figure 3(b) with Figure 8(f), samples TS2 and TS38 have similar porosity, but the clay content of the former is much higher and the conductivity lower than that of the latter (see Figures 5(b) and 10(f)), which may be related to $S_{e,1}$. Comparing samples TS19 and TS40, we find that the clay and siderite content of the two samples are almost the same (see Table 3), while the former contains a small amount of pyrite, but the corresponding $S_{e,1}$ is lower than that of the latter, indicating that the content of metallic minerals will not strongly affect the electrical conductivity. Samples TS41 and TS42 allow the same conclusion.

Tables 2 and 4 show that the constant $m(n)$ of the tight sandstones of the Yanchang Formation is apparently lower than that of the Shaximiao one. According to the model, the permeability (conductivity) parameter m(n) is relevant to the properties of the soft part at low stresses. Comparing Figures 3–5 with Figures 8–10, the porosity variation of the former is smaller at low effective stresses as illustrated in the first figures, while the permeability variation has an opposite behavior, indicating that the m values of the former are higher. Similar discussions can be found in Dong et al. [63] (the corresponding m is high when the porosity change is small, while the permeability variation is high). Moreover, greater porosity may lead to more electrical paths, and we have found that $S_{e,1}$ increases with increasing porosity $\phi_{e,1}$. In addition, it should be noted that the pore pressure is fixed in the experiment, and the effect of the effective stress is considered by changing the confining pressure. In rocks with low permeability, the Biot coefficient may be less than 1 [65], and furthermore, it has been considered that the Biot coefficient will basically decrease with the increase of effective stress [66, 67]. In this study, the Biot coefficient is assumed to be close to 1, which allows for reasonable predictions in the low-effective stress range, while deviations might exist for modeling at higher effective stresses. Liu et al. [46] assumed the Biot coefficient equals 1 when modeling sandstones for the porosity range of 9.00%–17.52% and the stress range of 0–100 MPa, and their predictions agree well with the measured results. In this work, according to the modeling results, the proposed procedure still provides satisfactory results in comparison with the measured data. Incorporating the effect of the variations in Biot coefficient in the approach of TPHM will be considered in future work.

5. Conclusions

The TPHM establishes the relation between the transport properties (permeability and electrical conductivity) and the effective stress of porous and fractured rocks. Experimental values of these properties and the porosity of tight sandstones from the Shaximiao and Yanchang Formations are employed in the analysis, and the results show that the

Table 4: Fitting parameters corresponding to the Yanchang Formation tight sandstones.

	$\Phi_{e,1}$ (%)	C_e (MPa^{-1})	$\gamma_{t,1}$ (%)	K_t (MPa)	$k_{e,1}$ (mD)	β	α (mD)	m	a	b (S/m)	$S_{e,1}$ (S/m)	n
TS18	4.89	1.84E-03	0.42	6.22	8.47E-04	1.38	2.40E-03	1.28	1.20	0.01	0.03	0.91
TS19	5.66	9.71E-04	0.43	5.07	7.04E-04	1.33	2.93E-03	1.04	1.11	0.01	0.01	1.11
TS27	6.64	9.79E-04	0.40	5.66	4.45E-03	4.66	2.83E-03	1.14	2.47	0.02	0.04	0.97
TS30	8.25	9.69E-04	0.26	7.32	6.69E-03	2.16	6.32E-02	1.42	1.62	0.05	0.04	1.66
TS35	8.70	7.47E-04	0.26	6.44	1.45E-02	1.94	9.08E-02	1.34	1.51	0.04	0.04	1.19
TS38	9.13	6.02E-04	0.32	5.49	1.38E-02	1.82	3.71E-02	1.12	1.47	0.02	0.05	0.77
TS40	4.83	1.55E-03	0.31	6.09	8.38E-04	1.03	1.69E-02	1.60	2.17	0.002	0.02	0.53
TS41	6.14	1.79E-03	0.79	5.91	6.54E-04	4.42	3.36E-03	1.54	1.16	0.007	0.03	1.05
TS42	7.11	5.62E-04	0.33	5.15	5.94E-03	4.67	3.03E-02	1.06	3.32	0.01	0.04	0.71

TPHM describes the experiments. The empirical exponential parameters of permeability and conductivity are similar, indicating that the effects of the cracks on the transport properties as a function of effective stress are similar. The analysis shows that the paths of fluid flow and electric current under are similar in the whole stress range. Cross-property relationship between conductivity and permeability will be developed in a future study, which can be used, for instance, to predict permeability from the resistivity log.

Data Availability

Datasets are available at https://zenodo.org/records/10526553

Conflicts of Interest

The authors declare that they have no conflict of interest.

Acknowledgments

This work is jointly funded by the National Natural Science Foundation of China (42104110, 12334019, and 42174161), Natural Science Foundation of Jiangsu Province (BK20210379), the Postdoctoral Science Foundation of China (2022M720989), Jiangsu Innovation and Entrepreneurship Plan.

References

[1] X. Tang, H. Wang, Y. Su, and X. Chen, "Inversion for micropore structure distribution characteristics using cracked porous medium elastic wave theory," *Chinese Journal of Geophysics*, vol. 64, no. 8, pp. 2941–2951, 2021.

[2] L. Zhang, J. Ba, and J. M. Carcione, "Wave propagation in infinituple-porosity media," *Journal of Geophysical Research*, vol. 126, no. 4, 2021.

[3] C. Ma, X. Zhao, T. Yang, et al., "Mineralogy, organic geochemistry, and microstructural characterization of lacustrine shahejie formation, Qikou sag, Bohai Bay basin: contribution to understanding microcosmic storage mechanism of shale oil," *Journal of Petroleum Science and Engineering*, vol. 209, p. 109843, 2022.

[4] A. Cardona, T. Finkbeiner, and J. C. Santamarina, "Natural rock fractures: from aperture to fluid flow," *Rock Mechanics and Rock Engineering*, vol. 54, no. 11, pp. 5827–5844, 2021.

[5] G. Mavko and D. Jizba, "Estimating grain-scale fluid effects on velocity dispersion in rocks," *GEOPHYSICS*, vol. 56, no. 12, pp. 1940–1949, 1991.

[6] M. Sahimi, "Flow phenomena in rocks: from continuum models to fractals, percolation, cellular automata, and simulated annealing," *Reviews of Modern Physics*, vol. 65, no. 4, pp. 1393–1534, 1993.

[7] A. Ebigbo, P. S. Lang, A. Paluszny, and R. W. Zimmerman, "Inclusion-based effective medium models for the permeability of a 3d fractured rock mass," *Transport in Porous Media*, vol. 113, no. 1, pp. 137–158, 2016.

[8] J. Guo, J. Germán Rubino, N. D. Barbosa, S. Glubokovskikh, and B. Gurevich, "Seismic dispersion and attenuation in saturated porous rocks with aligned fractures of finite thickness: theory and numerical simulations—part 1: P-wave perpendicular to the fracture planeFracture thickness and seismic signature," *GEOPHYSICS*, vol. 83, no. 1, pp. WA49–WA62, 2018.

[9] L. Zhang, J. Ba, J. M. Carcione, and W. T. Sun, "Modeling wave propagation in cracked porous media with penny-shaped inclusions penny-shaped inclusions," *GEOPHYSICS*, vol. 84, no. 4, pp. WA141–WA151, 2019.

[10] W. F. Brace, A. S. Orange, and T. R. Madden, "The effect of pressure on the electrical resistivity of water-saturated crystalline rocks," *Journal of Geophysical Research*, vol. 70, no. 22, pp. 5669–5678, 1965.

[11] J. R. Rice, "Fault stress states, pore pressure distributions, and the weakness of the san andreas fault,"in *In Fault Mechanics and Transport Properties of Rocks*, W. T.-f, Ed., pp. 475–503, Academic Press, 1992.

[12] J. P. Evans, C. B. Forster, and J. V. Goddard, "Permeability of fault-related rocks, and implications for hydraulic structure of fault zones," *Journal of Structural Geology*, vol. 19, no. 11, pp. 1393–1404, 1997.

[13] T. M. Daley, M. A. Schoenberg, J. Rutqvist, and K. T. Nihei, "Fractured reservoirs: an analysis of coupled elastodynamic and permeability changes from pore-pressure variation," *GEOPHYSICS*, vol. 71, no. 5, pp. O33–O41, 2006.

[14] M. Li, Y. Bernabé, W. -I. Xiao, Z. -Y. Chen, and Z. -Q. Liu, "Effective pressure law for permeability of E-bei sandstones," *Journal of Geophysical Research*, vol. 114, no. B7, 2009.

[15] S. A. Shapiro, G. P. Khizhniak, V. V. Plotnikov, R. Niemann, P. Y. Ilyushin, and S. V. Galkin, "Permeability dependency on stiff and compliant porosities: a model and some experimental examples," *Journal of Geophysics and Engineering*, vol. 12, no. 3, pp. 376–385, 2015.

[16] J. Sarout, E. Cazes, C. Delle Piane, A. Arena, and L. Esteban, "Stress-dependent permeability and wave dispersion in tight cracked rocks: experimental validation of simple effective medium models," *Journal of Geophysical Research*, vol. 122, no. 8, pp. 6180–6201, 2017.

[17] T. Han, "Joint elastic-electrical properties of artificial porous sandstone with aligned fractures," *Geophysical Research Letters*, vol. 45, no. 7, pp. 3051–3058, 2018.

[18] L. Zhang, J. Ba, and J. M. Carcione, "A rock-physics model to determine the pore microstructure of cracked porous rocks," *Geophysical Journal International*, vol. 223, no. 1, pp. 622–631, 2020.

[19] S. Al-Dughaimi, A. Muqtadir, T. Alzaki, and J. Dvorkin, "Stress dependence of elastic and transport properties in tight gas sandstones," *Journal of Petroleum Science and Engineering*, vol. 196, p. 108001, 2021.

[20] S. Q. Yang, P. F. Yin, and S. B. Xu, "Permeability evolution characteristics of intact and fractured shale specimens," *Rock Mechanics and Rock Engineering*, vol. 54, no. 12, pp. 6057–6076, 2021.

[21] C. David, T. F. Wong, W. L. Zhu, and J. X. Zhang, "Laboratory measurement of compaction-induced permeability change in porous rocks: implications for the generation and maintenance of pore pressure excess in the crust," *Pure and Applied Geophysics PAGEOPH*, vol. 143, nos. 1–3, pp. 425–456, 1994.

[22] J. Zheng, L. Zheng, H. H. Liu, and Y. Ju, "Relationships between permeability, porosity and effective stress for low-permeability sedimentary rock," *International Journal of Rock Mechanics and Mining Sciences*, vol. 78, pp. 304–318, 2015.

[23] J. E. Gale, "The effects of fracture type (induced versus natural) on the stress fracture closure-fracture permeability relationships,"in *Issues in rock mechanics, proceedings of 23rd US Symposium on Rock Mechanics*, Berkeley, California, 1982.

[24] J. H. Schön, "Physical properties of rocks: fundamentals and principles of petrophysics,"in *Handbook of Geophysical Exploration Section I, Seismic Exploration*. Vol. 18, 1996.

[25] Y. Shi and C. Y. Wang, "Pore pressure generation in sedimentary basins: overloading versus aquathermal," *Journal of Geophysical Research*, vol. 91, no. B2, pp. 2153–2162, 1986.

[26] S. Ghabezloo, J. Sulem, S. Guédon, and F. Martineau, "Effective stress law for the permeability of a limestone," *International Journal of Rock Mechanics and Mining Sciences*, vol. 46, no. 2, pp. 297–306, 2009.

[27] C. T. Gomez, J. Dvorkin, and T. Vanorio, "Laboratory measurements of porosity, permeability, resistivity, and velocity on fontainebleau sandstones," *GEOPHYSICS*, vol. 75, no. 6, pp. E191–E204, 2010.

[28] F. O. Jones and W. W. Owens, "A laboratory study of low-permeability gas sands," *Journal of Petroleum Technology*, vol. 32, no. 9, pp. 1631–1640, 1980.

[29] J. B. Walsh, "Effect of pore pressure and confining pressure on fracture permeability," *International Journal of Rock Mechanics and Mining Sciences & Geomechanics Abstracts*, vol. 18, no. 5, pp. 429–435, 1981.

[30] A. Kaselow and S. A. Shapiro, "Stress sensitivity of elastic moduli and electrical resistivity in porous rocks," *Journal of Geophysics and Engineering*, vol. 1, no. 1, pp. 1–11, 2004.

[31] J. Walder and A. Nur, "Porosity reduction and crustal pore pressure development," *Journal of Geophysical Research*, vol. 89, no. B13, pp. 11539–11548, 1984.

[32] Y. Bernabé, U. Mok, and B. Evans, "Permeability-porosity relationships in rocks subjected to various evolution processes," *Pure and Applied Geophysics*, vol. 160, nos. 5–6, pp. 937–960, 2003.

[33] G. E. Archie, "The electrical resistivity log as an aid in determining some reservoir characteristics," *Transactions of the AIME*, vol. 146, no. 1, pp. 54–62, 1942.

[34] H. S. Bao, T. C. Han, and L. Y. Fu, "Calculation method of digital rock electrical conductivity based on two-dimensional images," *Chinese J. Geophys*, vol. 64, no. 5, pp. 1733–1744, 2021.

[35] J. M. Carcione, "Theory and numerical simulation of wave propagation in anisotropic, anelastic, porous and electromagnetic media,"in *Wave Fields in Real Media*, (4th ed, rev), Elsevier, 2022.

[36] M. Pang, J. Ba, J. M. Carcione, E. H. Saenger, and S. Banham, "Elastic-electrical rock-physics template for the characterization of tight-oil reservoir rocks," *Lithosphere*, vol. 2021, no. Special 3, 2021.

[37] W. Al-Wardy and R. W. Zimmerman, "Effective stress law for the permeability of clay-rich sandstones," *Journal of Geophysical Research*, vol. 109, no. B4, 2004.

[38] T. Han, A. I. Best, J. Sothcott, L. J. North, and L. M. MacGregor, "Relationships among low frequency (2 Hz) electrical resistivity, porosity, clay content and permeability in reservoir sandstones," *Journal of Applied Geophysics*, vol. 112, pp. 279–289, 2015.

[39] L. D. Landau and E. M. Lifshitz, *Fluid Mechanics*, Pergamon, London, 1959.

[40] P. M. Doyen, "Permeability, conductivity, and pore geometry of sandstone," *Journal of Geophysical Research*, vol. 93, no. B7, pp. 7729–7740, 1988.

[41] T. F. Wong, J. T. Fredrich, and G. D. Gwanmesia, "Crack aperture statistics and pore space fractal geometry of westerly granite and Rutland quartzite: implications for an elastic contact model of rock compressibility," *Journal of Geophysical Research*, vol. 94, no. B8, pp. 10267–10278, 1989.

[42] L. J. Gelius and Z. Wang, "Modelling production caused changes in conductivity for a siliciclastic reservoir: a differential effective medium approach," *Geophysical Prospecting*, vol. 56, no. 5, pp. 677–691, 2008.

[43] M. Markov, A. Mousatov, and E. Kazatchenko, "Conductivity of carbonate formations with microfracture systems," *Journal of Petroleum Science and Engineering*, vol. 69, nos. 3–4, pp. 247–254, 2009.

[44] J. Sarout, "Impact of pore space topology on permeability, cut-off frequencies and validity of wave propagation theories," *Geophysical Journal International*, vol. 189, no. 1, pp. 481–492, 2012.

[45] L. Zhang, J. Ba, C. Li, J. M. Carcione, and F. Zhou, "Joint inversion of the pore geometry of tight sandstones based on elastic and electrical properties," *Journal of Petroleum Science and Engineering*, vol. 219, p. 111109, 2022.

[46] H. H. Liu, J. Rutqvist, and J. G. Berryman, "On the relationship between stress and elastic strain for porous and fractured rock," *International Journal of Rock Mechanics and Mining Sciences*, vol. 46, no. 2, pp. 289–296, 2009.

[47] J. C. Jaeger, N. G. W. Cook, and RW. Zimmerman, *Fundamentals of Rock Mechanics*. 4th ed, Oxford: Blackwell, 2007.

[48] Z. Wu, J. Zhang, X. Li, et al., "Influence of microcracks on stress sensitivity in tight sandstone," *Lithosphere*, vol. 2021, no. Special 4, 2021.

[49] Z. Y. Ye, J. H. Yang, F. Xiong, S. Huang, and A. Cheng, "Analytical relationships between normal stress and fluid flow for single fractures based on the two-part Hooke's model," *Journal of Hydrology*, vol. 608, p. 127633, 2022.

[50] J. Li, B. Li, Q. Cheng, and Z. Gao, "Evolution of anisotropic coal permeability under the effect of heterogeneous deformation of fractures," *Natural Resources Research*, vol. 30, no. 5, pp. 3623–3642, 2021.

[51] J. G. Wang, B. Hu, H. Liu, Y. Han, and J. Liu, "Effects of 'soft-hard' compaction and multiscale flow on the shale gas production from a multistage hydraulic fractured horizontal well," *Journal of Petroleum Science and Engineering*, vol. 170, pp. 873–887, 2018.

[52] H. H. Liu, M. Y. Wei, and J. Rutqvist, "Normal-stress dependence of fracture hydraulic properties including two-phase flow properties," *Hydrogeology Journal*, vol. 21, no. 2, pp. 371–382, 2013.

[53] L. C. Li and H. H. Liu, "A numerical study of the mechanical response to excavation and ventilation around tunnels in clay rocks," *International Journal of Rock Mechanics and Mining Sciences*, vol. 59, pp. 22–32, 2013.

[54] T. Watanabe, M. Makimura, Y. Kaiwa, G. Desbois, K. Yoshida, and K. Michibayashi, "Elastic wave velocity and electrical conductivity in a brine-saturated rock and microstructure of pores," *Earth, Planets and Space*, vol. 71, no. 1, pp. 1–12, 2019.

[55] M. Q. Pang, J. Ba, J. M. Carcione, M. Balcewicz, W. Z. Yue, and E. H. Saenger, "Acoustic and electrical properties of tight rocks: a comparative study between experiment and theory," *Surveys in Geophysics*, vol. 43, no. 6, pp. 1761–1791, 2022.

[56] J. B. Walsh and W. F. Brace, "The effect of pressure on porosity and the transport properties of rock," *Journal of Geophysical Research*, vol. 89, no. B11, pp. 9425–9431, 1984.

[57] W. F. Brace, J. B. Walsh, and W. T. Frangos, "Permeability of granite under high pressure," *Journal of Geophysical Research*, vol. 73, no. 6, pp. 2225–2236, 1968.

[58] K. B. Coyner, W. F. Brace, and J. B. Walsh, "New laboratory measurements of permeability and electrical resistivity of crystalline rocks," *Eos Trans AGU*, vol. 60, p. 943, 1979.

[59] M. S. Paterson, "The equivalent channel model for permeability and resistivity in fluid-saturated rock—a re-appraisal," *Mechanics of Materials*, vol. 2, no. 4, pp. 345–352, 1983.

[60] J. M. Carcione, B. Ursin, and J. I. Nordskag, "Cross-property relations between electrical conductivity and the seismic velocity of rocks," *GEOPHYSICS*, vol. 72, no. 5, pp. E193–E204, 2007.

[61] W. Wei, J. C. Cai, X. Y. Hu, and Q. Han, "An electrical conductivity model forfractal porous media," *Geophysical Research Letters*, vol. 42, no. 12, pp. 4833–4840, 2015.

[62] W. Z. Yue, G. Tao, X. Y. Chai, H. X. Jiang, and H. W. Mu, "Investigation of effects of clay content on F-Φ relationship by lattice gas automation using digital rock model," *Petroleum Science*, vol. 8, no. 2, pp. 170–176, 2011.

[63] J. J. Dong, J. Y. Hsu, W. J. Wu, et al., "Stress-dependence of the permeability and porosity of sandstone and shale from TCDP hole-A," *International Journal of Rock Mechanics and Mining Sciences*, vol. 47, no. 7, pp. 1141–1157, 2010.

[64] J. M. Carcione, G. Seriani, and D. Gei, "Acoustic and electromagnetic properties of soils saturated with salt water and NAPL," *Journal of Applied Geophysics*, vol. 52, no. 4, pp. 177–191, 2003.

[65] X. D. Ma and M. D. Zoback, "Laboratory experiments simulating poroelastic stress changes associated with depletion and injection in low-porosity sedimentary rocks," *Journal of Geophysical Research*, vol. 122, no. 4, pp. 2478–2503, 2017.

[66] Y. Wang, L. Jeannin, F. Agostini, L. Dormieux, F. Skoczylas, and E. Portier, "Experimental study and micromechanical interpretation of the poroelastic behaviour and permeability of a tight sandstone," *International Journal of Rock Mechanics and Mining Sciences*, vol. 103, pp. 89–95, 2018.

[67] G. Blöcher, T. Reinsch, A. Hassanzadegan, H. Milsch, and G. Zimmermann, "Direct and indirect laboratory measurements of poroelastic properties of two consolidated sandstones," *International Journal of Rock Mechanics and Mining Sciences*, vol. 67, pp. 191–201, 2014.